

Time scale stability analysis of a Hopf bifurcation in a wind-diesel hybrid microgrid

ISSN 1752-1416 Received on 18th October 2019 Revised 22nd February 2020 Accepted on 9th March 2020 E-First on 7th May 2020 doi: 10.1049/iet-rpg.2019.1193 www.ietdl.org

Edwin Choque Pillco^{1 \to 1}, Luís Fernando Costa Alberto², Ricardo Vasques de Oliveira¹

¹Electrical Engineering Department, Federal University of Technology (Paraná), Via do Conhecimento km 1 CEP: 85503-390, Pato Branco, PR, Brazil

Abstract: Microgrids and modern bulk power systems usually have multiple time scale dynamics, such as slow and fast dynamics. In this study, the stability of a wind–diesel hybrid microgrid is investigated to show a mechanism of system collapse caused by the interaction between fast dynamics of interface converters and slow electromechanical dynamics. This mechanism leads to a Hopf bifurcation of the fast subsystem due to slow changes in the variables of the slow subsystem and is completely understood by decomposing the stability analysis of the microgrid into the stability assessment of two simpler subsystems: the slow and the fast subsystems. The time-scale method proposed in this study for stability analysis of the microgrid extends the existing proposals in the literature and is able to detect this kind of instability scenario, where the interaction between fast and slow subsystems is the cause of collapse, while the existing approaches, such as quasi-steady-state analysis, fail in detecting instability.

Nomenclature

Acronyms

QSS quasi steady-state
WECS wind energy conversion systems
DERs distributed energy resources
ASEP asymptotically stable equilibrium point
differential algebraic equations
FRC fully rated converter

PQ active and reactive power LS load-side

GS generator-side V-f voltage—frequency

MPPT maximum power point tracking

PLL phased-locked loop

CUEP controlling unstable equilibrium point

SR stability region

Symbols

7.

 $egin{array}{ll} U_i & & \mbox{dynamical system } i \ \Sigma_{\mathcal{E}} & & \mbox{singularly perturbed system} \ \Sigma_{\mbox{o}} & & \mbox{slow subsystem} \ \Pi_{\mbox{F}} & & \mbox{fast subsystem} \ x & & \mbox{slow dynamics} \ \end{array}$

fast dynamics

 φ_0 trajectory of the slow subsystem Φ_0 trajectory of the fast subsystem (x_s, z_s) asymptotically stable equilibrium point

 $A_i(x_s, z_s)$ stability region of (x_s, z_s)

 $\begin{array}{ll} (x_{i-1},z_{i-1}) & \text{start point of the trajectory of } U_i \\ (x_{i-1},z_{i-1}^*) & \text{ASEP of the fast subsystem of } U_i \\ (x_{si}^{U_i},z_{si}^{U_i}) & \text{ASEP of the slow subsystem of } U_i \\ \end{array}$

 ε small positive number t time in seconds τ scaled time (t/ε)

large positive number (infinite)
 constraint of the slow dynamics
 derivative with respect to time (d/dt)

 $\begin{array}{ccc} \delta & & \text{load angle} \\ \omega & & \text{angular speed} \\ \Delta & & \text{variation} \end{array}$

Subscripts

F fast subsystem o slow subsystem

w wind tur turbine dg diesel generator

asymptotically stable equilibrium point

L load

Superscripts

 U_i dynamical system i

1 Introduction

Modern power systems are undergoing significant changes in terms of energy sources and structure, with clear benefits in economics and environmental aspects, but with an increasing complexity in operational procedures and dynamic analysis. Renewable energy sources have been attracting great attention due to the cost increase, limited reserves and adverse environmental impacts of fossil fuels [1]. Wind energy conversion systems (WECS), for example, are increasingly becoming mainstream and competitive with conventional generation [2, 3].

Microgrids are also receiving widespread attention, since they are an attractive alternative to manage distributed energy resources (DERs) in order to ensure security, power quality, energy efficiency and reliability for critical loads [4]. Many of the DERs are nonconventional forms of energy generation that require the employment of static converters to enable their connection with the grid. WECS, for example, often employ static converters to control the active and reactive power injected into the grid [5]. AC/DC hybrid power systems are becoming common at the level of transmission and distribution.

Hybrid power systems have more complex dynamics than conventional AC power systems [6-8] and new scenarios of

instability have emerged due to the interaction among dynamics of interface converters and electromechanical dynamics. Consequently, there is a need for understanding the mechanisms that may lead hybrid power systems to instability. In the context of hybrid systems, this paper investigates the stability of a wind-diesel hybrid microgrid, which modelling and control performance was analysed in [9]. Particularly, a special scenario of unstable interaction of the fast dynamics of the DC-link controller and load-side converter of the wind generation unit with the slow electromechanical dynamics is investigated.

Dynamics with different time scales coexist in power systems, mainly in hybrid power systems. Hence, exploring time scale features in the stability analysis of AC/DC hybrid power systems [6, 10] provides a deeper and comprehensive understanding of their dynamics. In this context, a time-scale algorithm, which is an extension of the method proposed in [11], is proposed in this paper and employed to investigate the aforementioned unstable scenario of a wind–diesel hybrid microgrid. This time-scale algorithm offers a comprehensive understanding of the mechanisms of collapse of the hybrid microgrid by decomposing the stability analysis into the stability analysis of simpler systems: the slow and the fast subsystems.

Decomposing the stability analysis of complex hybrid power systems in time-scales has several advantages. The time scale approach does not require numerical integration of the complete dynamical model, which mitigates the occurrence of numerical instability due to the coexistence of dynamics in very different time ranges [10, 12]. Hence, an appropriate choice of integration time steps for the slow and fast dynamics has the potential to speed up the analysis, reducing errors introduced by conventional algorithms.

The decomposition of the analysis in time-scales also offers a comprehensive understanding of the mechanisms of collapse of the hybrid microgrid. A proper classification of the system dynamics into fast and slow dynamics facilitates the observation of the interaction and evolution of dynamics of every component of the microgrid, providing not only an effective stability assessment but also a much deeper insight into the mechanisms of collapse of the microgrid and the devices involved in these mechanisms.

In the particular studied scenario, time scale decomposition clearly indicates the occurrence of a Hopf bifurcation in the fast subsystem, which includes dynamics of interface converters, induced by slow changes in the slow state variables.

The contributions of this paper are:

- A comprehensive analysis, via time-scale method, of a scenario of instability of a hybrid wind-diesel microgrid caused by the interaction between fast dynamics of the interface converters and electromechanical dynamics.
- ii. The proposal of an extension of the time scale algorithm proposed in [11] for stability analysis of power systems. The proposed scheme splits the stability analysis of a power system, bridging the gap between short and mid-term stability analysis.

Also, the theoretical foundations developed in [11] are further extended in this paper, in order to ensure that all possible fast and slow unstable dynamics of a power system are captured in the analysis. Particularly, the foundations to detect the onset of instability caused by bifurcations in the fast subsystem due to slow changes in the slow subsystem state variables are developed.

Although the idea of decomposition of stability analysis is not new in the literature of power systems [13, 14], the proposed algorithm integrates short and mid-term stability analysis into a single algorithm, which has transient stability and QSS analysis [10, 11, 15–17] as particular cases. Based on the singular perturbation and stability region theory [15, 17], the method captures instability scenarios which are consequence of interaction between fast and slow dynamics avoiding erroneous conclusions about stability when transient stability analysis and QSS analysis are separately performed.

This paper shows that QSS method fails to detect the unstable scenario of the studied hybrid wind-diesel microgrid while the proposed time-scale algorithm captures it and provides a clear understanding of the collapse mechanisms, which is crucial for engineers to design preventive or corrective actions.

The paper is organised as follows. Section 2 reviews the basic concepts about time scale decomposition, briefly describes the general time scales criteria for stability analysis and the proposed approach for decomposing stability analysis in time scales. In Section 3, the wind generation based microgrid model is presented and the time scale classification of its dynamics is addressed. In Section 4, the proposed time scale algorithm is applied to the stability analysis of a wind–diesel hybrid microgrid to explain the mechanisms of a particular unstable scenario caused by the interaction between fast dynamics of converters and slow dynamics of the power system. The conclusions and future works are discussed in Section 5.

2 Time scale decomposition for stability analysis

Assume the electrical power system can be represented, in the form of a singularly perturbed system, by

$$(\Sigma_{\varepsilon}) \begin{cases} \frac{\mathrm{d}x}{\mathrm{d}t} = f(x, z) \\ \varepsilon \frac{\mathrm{d}z}{\mathrm{d}t} = g(x, z) \end{cases}$$
 (1)

with $\varepsilon > 0$ being a small real number, $\mathbf{x} \in R^n$ a vector of slow dynamics, $\mathbf{z} \in R^m$ a vector of fast dynamics, $\mathbf{f}: R^n \mathbf{x} R^m \to R^n$ and $\mathbf{g}: R^n \mathbf{x} R^m \to R^m$ functions of class C^1 . We denote $\varphi_{\varepsilon}(t, \mathbf{x}_0, \mathbf{z}_0)$ as the trajectory of (Σ_{ε}) starting in $(\mathbf{x}_0, \mathbf{z}_0)$. Let $(\mathbf{x}_s, \mathbf{z}_s)$ be an asymptotically stable equilibrium point (ASEP) of (1), then $A_{\varepsilon}(\mathbf{x}_s, \mathbf{z}_s) = \{(\mathbf{x}, \mathbf{z}) \in R^n \times R^m : \varphi_{\varepsilon}(t, \mathbf{x}, \mathbf{z}) \to (\mathbf{x}_s, \mathbf{z}_s) \text{ as } t \to \infty\}$ is the stability region of $(\mathbf{x}_s, \mathbf{z}_s)$.

Letting $\varepsilon \to 0$ in (1), we obtain the slow subsystem (Σ_0), represented by the following set of differential algebraic equations:

$$(\Sigma_o) \begin{cases} \frac{\mathrm{d}x}{\mathrm{d}t} = f(x, z) \\ 0 = g(x, z) \end{cases}$$
 (2)

The algebraic equation 0 = g(x, z) constrains the slow dynamics of (2) to a set Γ in R^{n+m} , defined as $\Gamma = \{(x,z) \in R^n \times R^m \colon \mathbf{0} = g(x,z)\}$. Set Γ is an invariant set with respect to the slow system (Σ_0) . We denote $\varphi_0(t,x_0,z_0)$ as the trajectory of the slow subsystem (Σ_0) starting in $(x_0,z_0) \in \Gamma$ and $A_0 = \{(x,z) \in \Gamma \colon \varphi_0(t,x_0,z_0) \to (x_s,z_s) \text{ as } t \to \infty\}$ as the stability region of the ASEP (x_s,z_s) related to the slow system (Σ_0) .

Letting $\tau = t/\varepsilon$, the time is scaled and the system (\sum_{ε}) in (1) takes the form

$$(\Pi_{\varepsilon}) \begin{cases} \frac{\mathrm{d}x}{\mathrm{d}\tau} = \varepsilon f(x, z) \\ \frac{\mathrm{d}z}{\mathrm{d}\tau} = g(x, z) \end{cases}$$
 (3)

Letting $\varepsilon \to 0$ in (Π_{ε}) , we obtain the fast subsystem (Π_F) , where x is frozen. The fast subsystem can be viewed as a family of systems parameterised in the variable x

$$(\Pi_{\rm F}(x)) \left\{ \begin{array}{l} \frac{{\rm d}z}{{\rm d}\tau} = g(x,z) \end{array} \right. \tag{4}$$

where x is frozen and treated as a parameter. Observe that (x,z) is an equilibrium point of the fast subsystem $(\Pi_F(x))$ if and only if $(x,z) \in \Gamma$. We denote $\Phi_0 := (\tilde{x}(\tau) \equiv x_0, \tilde{z}(\tau, x_0, z_0))$ as the trajectory of (Π_F) starting in (x_0,z_0) , where $\tilde{z}(\tau,x_0,z_0)$ is the solution of $(\Pi_F(x_0))$ starting in z_0 for $z=x_0$, and $A_F(x_0,z^*)=\{z\in R^m: \Phi_0(\tau,x_0,z)\to (x_0,z^*) \text{ as } \tau\to\infty\}$ as the stability region of (x_0,z^*) relative to the fast subsystem $(\Pi_F(x_0))$ when $z=x_0$ is frozen.

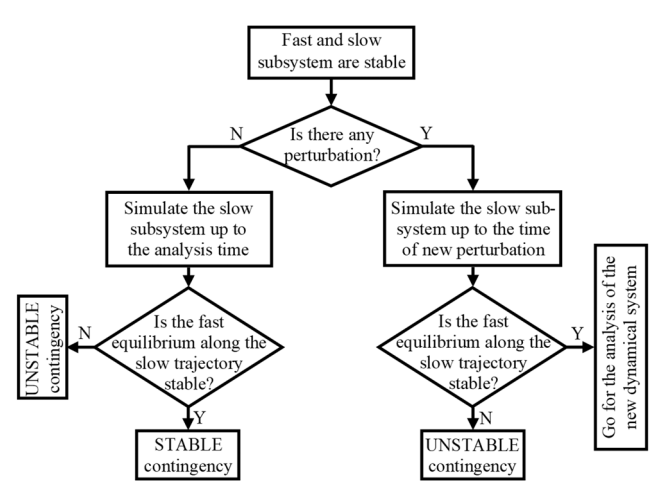


Fig. 1 Algorithm to detect bifurcations of the fast subsystem due to changes in the slow state variables

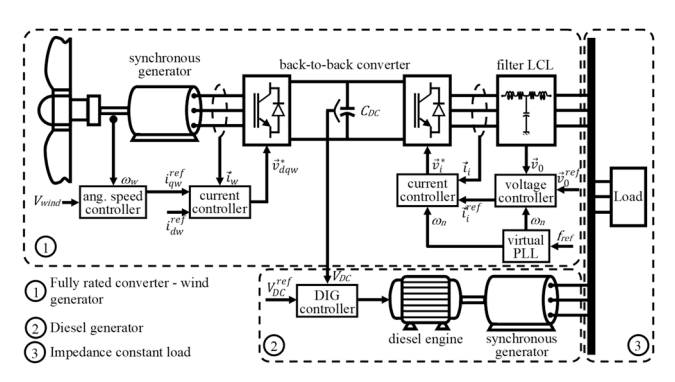


Fig. 2 Wind-diesel hybrid microgrid, proposed in [9]

The time scale decomposition method proposed in [11] is established under the generic assumption that all the equilibrium points of the singularly perturbed system (\sum_{ϵ}) are hyperbolic and every bounded trajectory approaches an equilibrium point [18]. Indeed, time scale decomposition is based on the following three main assumptions regarding the decomposition of stability analysis in time scales:

Assumption 1: Stability of the fast and slow subsystem implies stability of the two-time scale system.

Assumption 2: Instability of the fast subsystem implies instability of the two-time scale system.

Assumption 3: Instability of the slow subsystem implies instability of the two-time scale system.

Assumption 1, proven in [11], establishes that the conclusion of stability of the fast subsystem (Π_F) together with the conclusion of stability of the slow subsystem (Σ_0) implies stability of the original singularly perturbed system (Σ_{ϵ}) for sufficiently small ϵ . The proof of validity of Assumption 2, which corresponds to one of the contributions of this work, is proven in Appendix 1 (Theorem 1). It establishes that the instability of the fast subsystem (Π_{F}) implies instability of the original singularly perturbed system (Σ_{ε}) . In other words. Assumption 2 implies that if the initial condition of the fast subsystem is outside the stability region of the fast subsystem, then either the initial condition of the original system is outside the stability region of the original system or the state variables of the original system reach unacceptable large values for sufficiently small ε . The proof of validity of Assumption 3 is similar to the proof of Assumption 2 and will be omitted. It establishes that the conclusion of instability of the slow subsystem (Σ_0) implies instability of the original singularly perturbed system (Σ_{ε}) for sufficiently small ε . In other words, Assumption 3 implies that if the initial condition of the slow subsystem is outside the stability region of the stable equilibrium point, then either the initial condition of the original system is outside the stability region of the

original system or the state variables of the original system reach unacceptable large values for sufficiently small ε .

The proposed algorithm for decomposing stability analysis of a power system in [11] assumes that after a fault, a switch or a perturbation, a new dynamical system is originated. The stability analysis of each new dynamical system in time scales always starts with the stability assessment of the fast subsystem. If the fast subsystem is stable, then the stability of the slow subsystem is checked. If both subsystems are stable, then Assumption 1 guarantees the stability of the original dynamical system. However, two further conditions still have to be verified to ensure system stability: (i) there are no further perturbations or switching and (ii) no bifurcations of the fast equilibrium occur due to the variation of the slow dynamics up to the time of interest in the analysis. The algorithm proposed in [11] does not check condition (ii).

As an extension of the algorithm proposed in [11], the algorithm illustrated in Fig. 1 is proposed in this paper to detect the occurrence of bifurcations of the fast subsystem induced by slow dynamics. When the algorithm proposed in [11] indicates stability of the fast and slow subsystem, then the algorithm of Fig. 1 is applied. In case of no new perturbation occurrences and no occurrence of bifurcations of the fast equilibrium up to the time analysis, then the original dynamical system is stable. If a bifurcation of the fast equilibrium is detected up to the time of analysis, then the dynamical system is unstable.

3 Wind generation based microgrid: system structure and modelling

The microgrid considered in this paper, depicted in Fig. 2, is a stand-alone hybrid system composed of three main components: (1) a wind generation unit based on fully rated converter (FRC); (2) a diesel generator; (3) a single load, modelled as constant impedance [9]. The wind generation unit is composed of: (i) a wind turbine, (ii) a synchronous generator, (iii) a back-to-back converter and (iv) a LCL filter. Details about the modelling of components (i) and (ii) are found in [5]. The microgrid operating in the isolated mode (or, equivalently, stand-alone mode) is more susceptible to instability than operating in the on-grid mode due to the typical relatively small capacity and intermittent nature of distributed generation units [19]. Owing to this inherent dynamic vulnerability, the isolated mode is a more interesting case and was chosen for analysis in this work. Despite that, it is important to remark that the time scale approach employed to assess the system stability is general and can be applied to study stability of both grid-connected and isolated microgrids. Hybrid AC/DC power systems, in particular wind-diesel hybrid systems, have multi-time scale features [20, 21]. In this section, schematics and block control diagrams of the main components of the considered microgrid are shown.

The back-to-back converter and the LCL filter are represented by average models [1, 5]. The synchronous generator is equipped with a first-order voltage regulator [5] and the back-to-back converter has controllers in both sides, load-side (LS) and generator-side (GS). Fig. 3 depicts the LS control loops, which operates in voltage—frequency (V–f) control mode [22].

Fig. 4 depicts the GS control loops, which operates controlling the stator currents of the synchronous generator of the wind unit based on the maximum power point tracking (MPPT) strategy [23, 24]. The diesel unit, which operates in PQ control mode delivering active and reactive power, is composed of a synchronous generator with a first-order voltage regulator, as detailed in [5].

The mechanical power (P_{mdg}) of the synchronous generator comes from a diesel engine represented by a first-order model [25]. Since the wind unit operates in V-f control model, the control of the DC-link voltage (V_{DC}) of the unit is carried out by means of the diesel unit, based on the control strategy proposed in [9]. Fig. 5 depicts the control loop employed to control the DC-link voltage of the wind unit by means of the diesel unit.

The model of the hybrid microgrid is represented by the set of non-linear differential equations (5)–(28), (Σ_{ϵ}), with 28 state variables, where the prime (') indicates derivative with respect to time (d/dt)

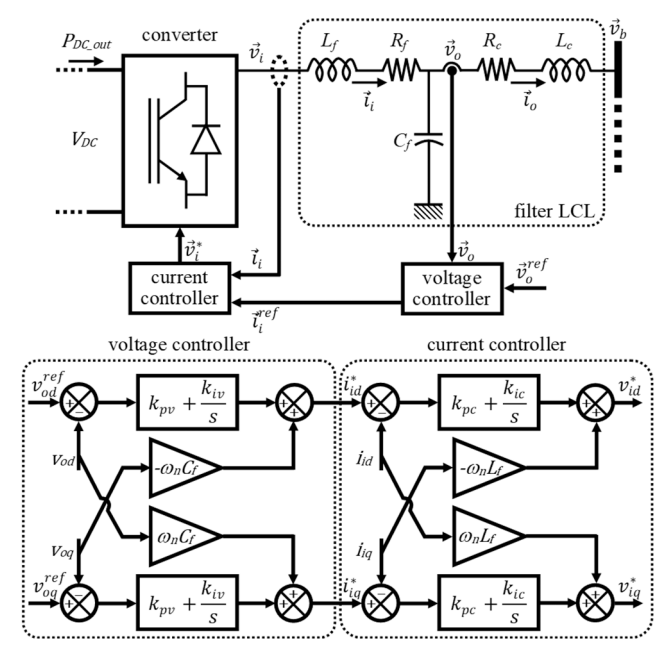


Fig. 3 Schematic and block diagrams of the control loops of the LS Converter

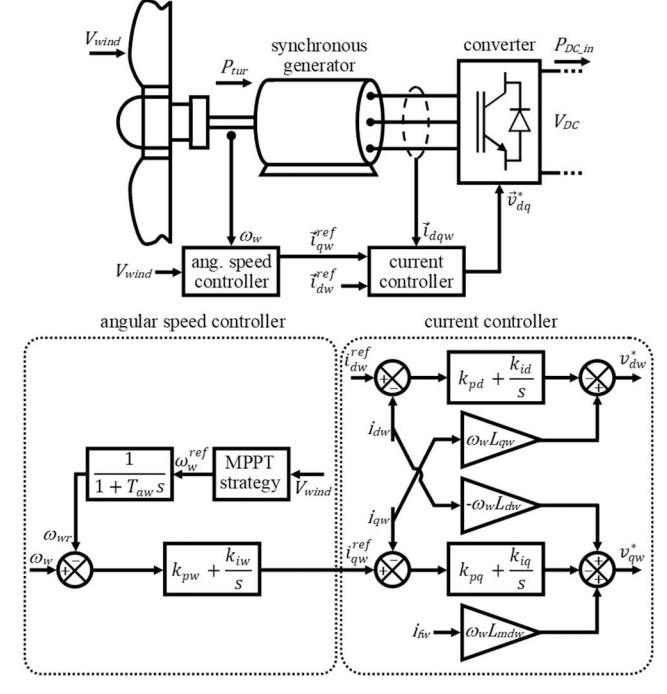


Fig. 4 Schematic and block diagrams of the control loop of the GS converter

$$U'_{e\omega w} = \omega_w - \omega_{wr} \tag{5}$$

$$U'_{eidw} = i_{dw}^{\text{ref}} - i_{dw} \tag{6}$$

$$U'_{eiaw} = i^{ref}_{aw} - i_{aw} \tag{7}$$

$$\omega'_{wr} = \frac{1}{T_{aw}} (\omega_w^{\text{ref}} - \omega_{wr})$$
 (8)

$$\omega_w' = \frac{S_b}{J_{tur}\omega_{mb}^2} \left(\frac{P_{tur}}{\omega_w} - T_{ew} \right) \tag{9}$$

$$E'_{fdw} = \frac{1}{T_{rw}} (K_{rw} (v_w^{\text{ref}} - v_w) - E_{fdw})$$
 (10)

$$\begin{bmatrix} i'_{dw} \\ i'_{qw} \\ i'_{fw} \end{bmatrix} = \omega_{eb} A_w^{-1} \begin{bmatrix} v_{dw}^* \\ v_{qw}^* \\ v_{fw} \end{bmatrix} - (M_w + N_w A_w) \begin{bmatrix} i_{dw} \\ i_{qw} \\ i_{fw} \end{bmatrix}$$
(11)

$$U'_{e\text{VDC}} = V_{\text{DC}}^{\text{ref}} - V_{\text{DC}} \tag{12}$$

$$V'_{\rm DC} = \frac{\omega_b}{C_{\rm DC}V_{\rm DC}}(P_{\rm DC_in} - P_{\rm DC_out})$$
 (13)

$$P'_{mdg} = \frac{1}{T_{amd}} (P_{\text{DGI0}} + A_{\text{DGI}} - P_{mdg})$$
 (14)

$$\delta_{dg}' = \omega_b(\omega_{dg} - 1) \tag{15}$$

$$\omega'_{dg} = \frac{1}{2H} (P_{mdg} - P_{edg} - D(\omega_{dg} - 1))$$
 (16)

$$U'_{evod} = v_{od}^{\text{ref}} - v_{od} \tag{17}$$

$$U'_{evog} = v_{og}^{\text{ref}} - v_{og} \tag{18}$$

$$U'_{eiid} = i_{id}^* - i_{id} \tag{19}$$

$$U'_{eiiq} = i_{iq}^* - i_{iq} (20)$$

$$i'_{id} = \left(\frac{\omega_b}{L_f}\right) \left(-R_f i_{id} + L_f \omega_n i_{iq} + v_{id}^* - v_{od}\right)$$
 (21)

$$i'_{iq} = \left(\frac{\omega_b}{L_f}\right) \left(-R_f i_{iq} + L_f \omega_n i_{id} + v_{iq}^* - v_{oq}\right)$$
 (22)

$$v'_{od} = \left(\frac{\omega_b}{L_f}\right) \left(\omega_n C_f v_{oq} + i_{id} - i_{od}\right)$$
 (23)

$$v'_{oq} = \left(\frac{\omega_b}{L_f}\right) \left(-\omega_n C_f v_{od} + i_{iq} - i_{oq}\right)$$
 (24)

$$i'_{od} = \left(\frac{\omega_b}{L_c}\right) \left(-R_c i_{od} + \omega_n L_c i_{oq} + v_{od} - v_{bd}\right)$$
 (25)

$$i'_{oq} = \left(\frac{\omega_b}{L_c}\right) \left(-R_c i_{oq} - \omega_n L_c i_{od} + v_{oq} - v_{bq}\right)$$
 (26)

$$E'_{fddg} = \frac{1}{T_{ei}} \left(k_{ei} \left(Q_{dg}^{ref} - Q_{dg} \right) - E_{fddg} \right) \tag{27}$$

$$\begin{bmatrix} i'_{ddg} \\ i'_{qdg} \\ i'_{fdg} \end{bmatrix} = \omega_b A_{dg}^{-1} \begin{bmatrix} v_{ddg} \\ v_{qdg} \\ v_{fdg} \end{bmatrix} - \left(M_{dg} + N_{dg} A_{dg} \right) \begin{bmatrix} i_{ddg} \\ i_{qdg} \\ i_{fdg} \end{bmatrix}$$
(28)

3.1 Classification of the microgrid dynamics

In the context of time scale analysis, the system dynamics must be split into slow and fast dynamics. The angular speed of the wind turbine (ω_w) and its speed reference (ω_{wr}) are classified as slow dynamics, due to the high inertia of the wind turbine. The d-axis voltage of the synchronous generator of the wind unit $(E_{fdw} = \omega_w L_{mdw} v_{fw}/r_{fw})$ has a direct dependence on the angular speed of the wind turbine (ω_w) [5], and for this reason, it is classified as a slow dynamic. According to the set of equations (11), the time derivative of the wind generator currents (i_{dw}, i_{qw}, i_{fw}) depends on ω_w , and, therefore, these currents are also classified as slow dynamics.

The dynamics associated with the diesel generator are P_{mdg} , δ_{dg} , ω_{dg} , E_{fddg} , i_{ddg} , i_{qdg} , i_{fdg} . The mechanical power from the prime mover (P_{mdg}) is classified as a slow dynamic, due to the inertial nature of the diesel engine and its dependence on other slow dynamics. However, ω_{dg} , E_{fddg} , i_{ddg} , i_{fdg} , i_{fdg} are classified as

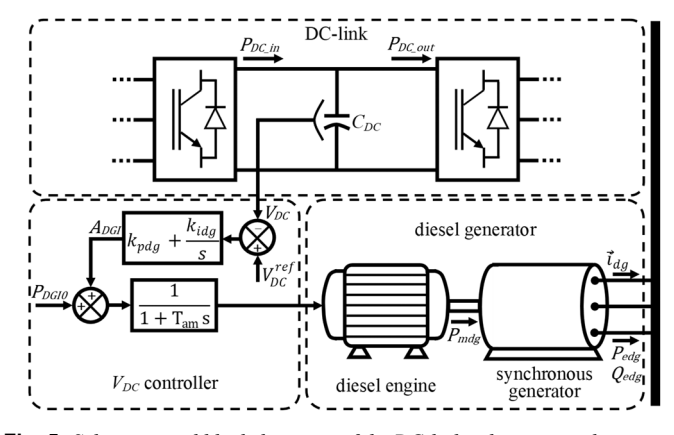


Fig. 5 Schematic and block diagrams of the DC-link voltage control

fast dynamics because the frequency at the load side of the microgrid is controlled by a virtual phased-locked loop added to the static converter, which, according to the set of equations (16), (27) and (28), have a fast rate of change.

The time scale decomposition for the load angle of the diesel generator (δ_{dg}) is a special case. Due to the explicit dependence of its vector field on the fast dynamics related to ω_{dg} , it possesses fast features. But also, due to (16), this variable (δ_{dg}) exhibits slow dynamics. Thus, the dynamic representation of the variable δ_{dg} will be maintained in both subsystems (slow and fast one). Thereby, scaling the time by $\tau = t/\varepsilon$, where ε is a small and positive constant, we get the fast time evolution of δ_{dg} and ω_{dg} from (15) and (16), given by

$$\frac{\mathrm{d}\delta_{dg}^{f}}{\mathrm{d}\tau} = \varepsilon \omega_{b}(\omega_{dg} - 1)$$

$$\frac{\mathrm{d}\omega_{dg}}{\mathrm{d}\tau} = \frac{\varepsilon}{2H}(P_{mdg} - P_{edg} - D(\omega_{dg} - 1))$$
(29)

To recover the slow evolution of δ_{dg} , which we denote δ_{dg}^{s} , we take $d\omega_{dg}/dt = 0$ in (16), obtaining the following representation for the slow subsystem:

$$\frac{d\delta_{dg}^{s}}{dt} = \omega_{b}(\omega_{dg} - 1)$$

$$0 = P_{mdg} - P_{edg} - D(\omega_{dg} - 1)$$
(30)

In the sequence, the voltage in the DC-link (V_{DC}) [5], depicted in Fig. 5, was classified as a slow dynamic because of the high capacitance of the DC-link. The variables from controllers associated with slow dynamics are also classified as slow ones. These controllers are the wind turbine angular speed controller and current controller, presented in Fig. 4, voltage controller of the wind generator and $V_{\rm DC}$ controller, presented in Fig. 5. The control actions of such controllers are represented by the dynamics $U_{e\omega w}$, U_{eidw} , U_{eiqw} and U_{eVDC} presented in the corresponding set of equations (5), (6), (7) and (12). The remaining dynamics, which correspond to the current and voltages from the LCL filter and their controllers, are classified as fast ones according to [15]. Based on the previous classification of dynamics into slow and fast, the dynamical model of the wind microgrid set of equations (5)–(28), (Σ_{ε}) , is decomposed into its slow (Σ_{o}) and fast (Π_{F}) subsystems. The slow subsystem is represented by the set of equations as follows:

$$U'_{e\omega w} = \omega_w - \omega_{wr} \tag{31}$$

$$U'_{eidw} = i_{dw}^{\text{ref}} - i_{dw} \tag{32}$$

$$U'_{eiaw} = i^{\text{ref}}_{aw} - i_{aw} \tag{33}$$

$$\omega'_{wr} = \frac{1}{T_{ow}} \left(\omega_w^{\text{ref}} - \omega_{wr} \right) \tag{34}$$

$$\omega_w' = \frac{S_b}{J_{tur}\omega_{mb}^2} \left(\frac{P_{tur}}{\omega_w} - T_{ew} \right)$$
 (35)

$$E'_{fdw} = \frac{1}{T_{rw}} \left(K_{rw} \left(v_w^{\text{ref}} - v_w \right) - E_{fdw} \right)$$
 (36)

$$\begin{bmatrix} i'_{dw} \\ i'_{qw} \\ i'_{fw} \end{bmatrix} = \omega_{eb} A_w^{-1} \begin{bmatrix} v_{dw}^* \\ v_{qw}^* \\ v_{fw} \end{bmatrix} - (M_w + N_w A_w) \begin{bmatrix} i_{dw} \\ i_{qw} \\ i_{fw} \end{bmatrix}$$
(37)

$$U'_{e\text{VDC}} = V_{\text{DC}}^{\text{ref}} - V_{\text{DC}} \tag{38}$$

$$V'_{\rm DC} = \frac{\omega_b}{C_{\rm DC}V_{\rm DC}} (P_{\rm DC_in} - P_{\rm DC_out})$$
 (39)

$$P'_{mdg} = \frac{1}{T_{amd}} (P_{\text{DGI0}} + A_{\text{DGI}} - P_{mdg}) \tag{40}$$

$$\delta_{dg}^{s'} = \omega_b(\omega_{dg} - 1) \tag{41}$$

$$0 = g(z, x) \tag{42}$$

The fast subsystem is described by the set of equations as follows:

$$\delta_{dg}^{f'} = \omega_b(\omega_{dg} - 1) \tag{43}$$

$$\omega'_{dg} = \frac{1}{2H} (P_{mdg} - P_{edg} - D(\omega_{dg} - 1))$$
 (44)

$$U'_{evod} = v_{od}^{\text{ref}} - v_{od} \tag{45}$$

$$U'_{evog} = v_{og}^{\text{ref}} - v_{og} \tag{46}$$

$$U'_{eiid} = i_{id}^* - i_{id} \tag{47}$$

$$U'_{eiiq} = i_{iq}^* - i_{iq} \tag{48}$$

$$i'_{id} = \left(\frac{\omega_b}{L_f}\right) \left(-R_f i_{id} + L_f \omega_n i_{iq} + v_{id}^* - v_{od}\right)$$
(49)

$$i'_{iq} = \left(\frac{\omega_b}{L_f}\right) \left(-R_f i_{iq} + L_f \omega_n i_{id} + v^*_{iq} - v_{oq}\right)$$
 (50)

$$v'_{od} = \left(\frac{\omega_b}{L_f}\right) \left(\omega_n C_f v_{oq} + i_{id} - i_{od}\right)$$
 (51)

$$v'_{oq} = \left(\frac{\omega_b}{L_f}\right) \left(-\omega_n C_f v_{od} + i_{iq} - i_{oq}\right)$$
 (52)

$$i'_{od} = \left(\frac{\omega_b}{L_c}\right) \left(-R_c i_{od} + \omega_n L_c i_{oq} + v_{od} - v_{bd}\right)$$
 (53)

$$i'_{oq} = \left(\frac{\omega_b}{L_c}\right) \left(-R_c i_{oq} - \omega_n L_c i_{od} + v_{oq} - v_{bq}\right)$$
 (54)

$$E'_{fddg} = \frac{1}{T_{ei}} \left(k_{ei} \left(Q_{dg}^{\text{ref}} - Q_{dg} \right) - E_{fddg} \right)$$
 (55)

$$\begin{bmatrix} i'_{ddg} \\ i'_{qdg} \\ i'_{fdg} \end{bmatrix} = \omega_b A_{dg}^{-1} \begin{bmatrix} v_{ddg} \\ v_{qdg} \\ v_{fdg} \end{bmatrix} - (M_{dg} + N_{dg} A_{dg}) \begin{bmatrix} i_{ddg} \\ i_{qdg} \\ i_{fdg} \end{bmatrix}.$$
 (56)

Table 1 Time scale classification of the dynamics of the hybrid system

slow dynamics (x)	$U_{e\omega w},~U_{eidw},~U_{eiqw},~\omega_{wr},~\omega_{w},~E_{fdw},~i_{dw},~i_{qw}, \\ i_{fw},~U_{eVDC},~V_{DC},~P_{mdg},~\delta^s_{dg}$	
fast dynamics (z)	δ_{dg}^{f} , ω_{dg} , U_{evod} , U_{evoq} , U_{elid} , U_{eliq} , i_{id} , i_{iq} , v_{od} , v_{od} , i_{od} , i_{od} , i_{od} , i_{od} , i_{dd} , i_{ddq} , i_{fdq}	

Table 2 Operational scenarios for the hybrid system

Time of occurrence	Operational event
unstable scenario 1	
<i>t</i> = 0 s	load increment in the system
<i>t</i> = 20 s	wind speed decreases
unstable scenario 2	
t=0 s	load increment in the system

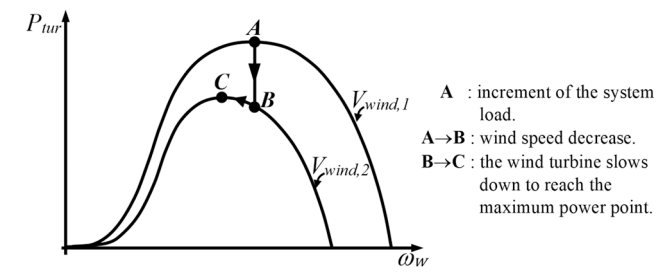


Fig. 6 Operational sequence for the wind turbine in scenario 1

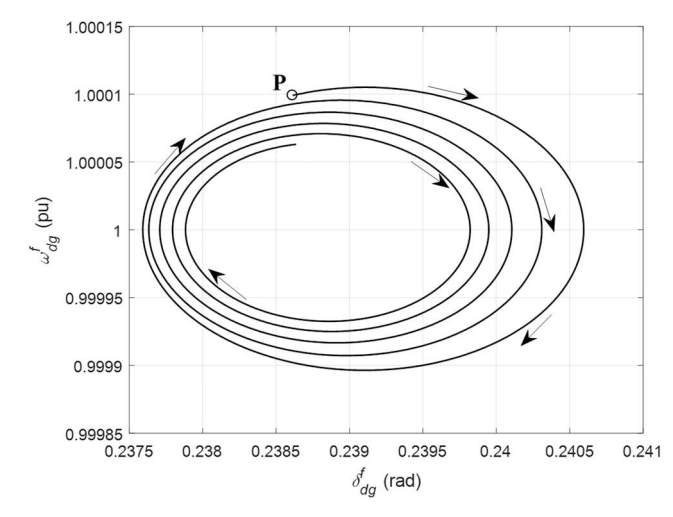


Fig. 7 Phase portrait δ - ω of the diesel generator corresponding to the fast subsystem of the dynamical system U_1

Table 1 summarises the classification of the microgrid dynamics into slow dynamics, represented by the state vector x, and fast dynamics, represented by the state vector z.

4 Time scale stability analysis of a hybrid winddiesel generation based microgrid

The general method for stability analysis in time scales described in Section 2 is applied to analyse stability of the stand-alone hybrid microgrid illustrated in Fig. 2. The nominal power of the diesel unit and wind power unit are 300 kW and 1.8 MW, respectively. The DC link of the wind power unit has a nominal voltage of 1.1 kV. The remaining data and parameters of the employed microgrid are presented in detail in [9]. It will be shown that the application of time scale analysis provides a deeper insight into the evolution of the microgrid dynamics, highlighting the collapse mechanisms of the microgrid. Table 2 summarises the two operational scenarios considered for stability assessment.

4.1 Stability assessment of scenario 1

Fig. 6 illustrates the operational scenario 1 via the power curve of the wind turbine, where $P_{\rm tur}$ is the power extracted by the wind turbine from the wind, ω_w is the wind turbine speed and $V_{\rm wind}$ is the wind speed.

4.1.1 Stability assessment by the time scale method: Employing the time scale method described in Section 2, two main perturbations are identified and, as a result, two dynamical systems are generated: U_1 , after the increase of the system load (ΔP_L = +58.15 kW), and U_2 , after the decrease of the wind speed ($\Delta V_{\rm wind}$ = -0.2 m/s).

The microgrid operates in steady state at an ASEP $(x_{0,1},z_{0,1})$ when, at t=0 s, it is subjected to a load increase (ΔP_L) equal to 58.15 kW, originating a new dynamical system (U_1) . Employing the time scale method described in [11] and Section 2, the analysis proceeds with the stability assessment of the fast subsystem U_1 . The ASEP of the fast subsystem, calculated by a Newton-Raphson algorithm taking $(x_{0,1},z_{0,1})$ as an initial guess, is $(x_{0,1},z_{0,1}^*)$. The values of all ASEPs are presented in Appendix 2.

Fig. 7 illustrates the stability behaviour of the fast subsystem by means of the phase portrait δ – ω . These dynamics correspond to the fast dynamics of the diesel unit. In the dynamical system U_1 , after the load increases, a voltage drop occurs at the load bus, which forces a sudden drop in v_0 and an increase in i_i . The variables v_0 and i_i , respectively, correspond to the voltage and current of the LCL filter. This voltage variation results in the action of the controllers of the LS converter and reactive power controller of the diesel generator in order to restore the system voltage. These voltage and current variations are fast dynamics related to $(\Pi_{F,1}^{U_1}(\mathbf{x}))$, which bring the microgrid from the point $(\mathbf{x}_{0,1}, \mathbf{z}_{0,1})$ to $(\mathbf{x}_{0,1}, \mathbf{z}_{0,1}^*)$. The fast subsystem was classified as stable and, as a consequence, the algorithm proceeds with the stability analysis of the slow subsystem U_1 .

The search for an ASEP of the slow system returns $(x_{s_1,1}^{U_1}, z_{s_1,1}^{U_1})$. The slow subsystem is classified as stable then the analysis proceeds to the proposed algorithm in Fig. 1. The slow subsystem evolution is related with the power unbalance at the DC-link, causing a slow variation in the DC-link voltage $(V_{\rm DC})$. The restoration of the DC-link voltage is a slow process, since this control process involves the action of the diesel engine, synchronous generator of the diesel unit and other components of the wind unit. The synchronous generator of the wind unit does not respond with a power increase, since the wind turbine operates at the maximum power point and cannot provide additional active power to the system. Thus, only the diesel unit supplies the deficit of energy to restore the voltage at the DC-link bus, which according to the time scale analysis is enough to recover the stability of the microgrid. Based on this analysis, the slow subsystem U_1 is classified as stable and the slow subsystem of U_1 , whose trajectory $(\boldsymbol{\varphi}_{0,1}^{U_1})$ is restricted to $\Gamma_{1,1}^{U_1}$: $\boldsymbol{g}_{1,1}(\boldsymbol{x},\boldsymbol{z}) = 0$, is numerically integrated up to t = 20 s (occurrence of the second perturbation), taking into account the ASEP $(x_{0,1}, z_{0,1}^*)$ of the fast subsystem as an initial condition for the slow trajectory. Then, the application of the algorithm of Fig. 1 does not indicate the occurrence of bifurcations of the equilibrium of the fast subsystem along the slow trajectory up to 20 s. The final state of U_1 at t = 20 s is $(x_{1,1},z_{1,1})$, which corresponds to the initial state of the dynamical system U_2 . After determining this initial state, then the analysis proceeds to the next perturbation.

At t = 20 s, the microgrid is subjected to a decrease of 0.2 m/s in the wind speed ($\Delta V_{\rm wind} = -0.2$ m/s), which originates the second dynamical system (U_2). This perturbation implies a decrease of the mechanical power extracted by the wind turbine ($P_{\rm tur}$) and stimulates fast and slow devices, such as the controllers at LS converter, voltage regulator of the diesel generator and the MPPT control of the wind unit. The time scale analysis of U_2 begins classifying its fast subsystem at t = 20 s as stable. The dynamics

Table 3 Fast subsystem eigenvalues of the dynamical system U_2 of scenario 1

Time		
24.45 s	24.50 s	24.55 s
-4947.84 + 34,555.79i	-4947.85 + 34,555.76i	-4947.86 + 34,555.72i
-4947.84 - 34,555.79i	-4947.85 - 34,555.76i	-4947.86 - 34,555.72i
-4899.12 + 34,130.40i	-4899.12 + 34,130.35i	-4899.12 + 34,130.30i
-4899.12 - 34,130.40i	-4899.12 - 34,130.35i	-4899.12 - 34,130.30i
-5985.46 + 1232.47i	-5985.45 + 1232.44i	-5985.45 + 1232.41i
-5985.46 - 1232.47i	-5985.45 - 1232.44i	-5985.45 - 1232.41i
-80.4224 + 369.722i	-80.4253 + 369.719i	-80.4279 + 369.718i
-80.4224 - 369.722i	-80.4253 - 369.719i	-80.4279 - 369.718i
-17.5535 + 49.7547i	-17.5561 + 49.7471i	-17.5589 + 49.7396i
-17.5535 - 49.7547i	-17.5561 - 49.7471i	-17.5589 - 49.7396i
-0.0014 + 30.3597i	0.0011 + 30.3697i	0.0036 + 30.3794i
-0.0014 - 30.3597i	0.0011 - 30.3697i	0.0036 - 30.3794i
-2.7257 + 0.0274i	-2.7257 + 0.0274i	-2.7257 + 0.0274i
-2.7257 - 0.0274i	-2.7257 - 0.0274i	-2.7257 - 0.0274i
-20.0171 + 0.0007i	-20.0171 + 0.0007i	-20.0171 + 0.0007i
-20.0171 - 0.0007i	-20.0171 - 0.0007i	-20.0171 - 0.0007i

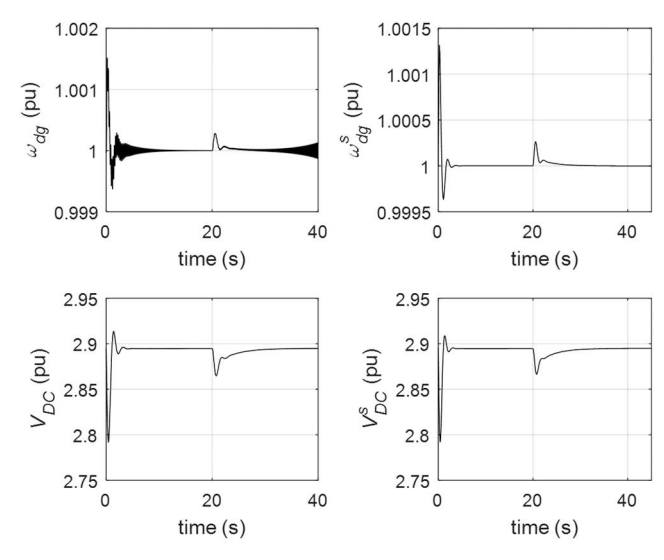


Fig. 8 Numerical simulation, left column: original singularly perturbed system $(\Sigma_{\mathcal{E}})$; right column: slow subsystem (Σ_0) (or QSS system)

involved in the fast subsystem are the voltage and current controllers located at the LS converter, which in conjunction with the voltage regulator of the diesel unit attempt to mitigate the voltage drop at the DC-link ($V_{\rm DC}$). The angle (δ_{dg}) and angular speed (ω_{dg}) variations of the synchronous generator at the diesel unit represent the transfer of active power promoted by the controller to restore the stability of the microgrid, which trajectory tends to the ASEP $(x_{1,1}, z_{1,1}^*)$. In the sequence, the slow subsystem is also classified as stable with an ASEP $(\mathbf{x}_{s2,1}^{U_2}, \mathbf{z}_{s2,1}^{U_2})$. A reduction in the wind speed implies the reduction of the mechanical power extracted by the wind turbine. Then, the angular speed controller at Fig. 4 and the voltage controllers of the DC-link at Fig. 5 are triggered, attempting to restore the voltage at the DC-link. Since both dynamical systems (fast and slow) are classified as stable, the algorithm proposed in Fig. 1 is applied to monitor the stability of the fast subsystem equilibrium along the trajectory of the slow subsystem ($\boldsymbol{\varphi}_{0,1}^{U_2}$).

The eigenvalues of the Jacobian matrix corresponding to the fast subsystem of U_2 are used as a tool to monitor the stability of the fast subsystem throughout the trajectory of the slow subsystem. At t = 24.5 s, this analysis shows, as presented in Table 3, that a pair of eigenvalues of the fast subsystem cross the imaginary axis of the complex plane to the right-hand semi-plane, indicating that the fast subsystem equilibrium becomes unstable. Thus, the

instability of the fast subsystem implies instability of the microgrid. It is worth remarking that in this case the QSS analysis (simulation of the slow subsystem) has failed in detecting the instability of the microgrid, while the proposed procedure has successfully identified the instability condition.

A comparison between dynamics obtained from numerical simulation of the complete dynamical system (Σ_{ε}) and obtained from the QSS system (Σ_0) is illustrated in Fig. 8. This comparison clearly shows how the QSS simulation leads to the wrong conclusion that the system is stable by assuming that the fast subsystem is stable during the entire period of analysis. By contrast, the time scale method identifies a Hopf bifurcation as a product of the interaction between slow and fast dynamics.

Fig. 9 shows the sequence of operational events of the microgrid in the context of time scales, pointing out the action of the controllers and devices related to the slow and fast subsystems of the corresponding dynamical systems U_1 and U_2 . The bifurcation detected at t = 24.5 s is known in the literature as a Hopf bifurcation point [26, 27]. Although this kind of instability is difficult to be detected by numerical methods [17, 28], since the analysis involves the behaviour of the eigenvalues of the complete dynamical system, the proposed time scale method has correctly detected it, showing that the unstable condition of the microgrid is related to the interaction of the fast dynamics of the DC-link controller and load-side converter of the wind generation unit with the slow electromechanical dynamics. This fact can be also verified by means of the phase portrait of the load angle (δ_{dg}) and angular speed (ω_{dg}) of the diesel generator illustrated in Fig. 10, which was obtained from time simulation of the complete dynamical model of the microgrid, represented by set of equations (5)-(28). As illustrated in the phase portrait presented at Fig. 10, after the sudden decrease of the wind speed (point P), the angular speed of the diesel generator temporarily increases and returns to the neighbourhood of its nominal value ($\omega_{dg} \simeq 1$, point Q). In fact, the fast action of the DC-link controller and controllers of the LS converter, which attempt to restore the power balance, manifests itself in the increase of the angular speed of the synchronous generator driven by diesel engine, leading the microgrid to instability. This occurs because the response of the synchronous generator of the diesel unit is not fast enough to keep the power balance required by the controllers as was clearly shown by the time scale analysis.

4.1.2 Stability assessment by the complete dynamical system: At the beginning, t=0 s, the system is subjected to a load increase $\Delta P_{\rm L}=+59.7$ kW. Since the wind turbine operates at its maximum power level, at point A of Fig. 6, only the diesel generator is able to pick up the load increase. The load increase results in a voltage drop at the DC-link ($V_{\rm DC}$), due to the power unbalance in the DC-link presented in Fig. 5. Large variations of the DC link voltage may trigger the protection system leading the system to a collapse. The $V_{\rm DC}$ controller, illustrated in Fig. 5, acts due to the DC voltage variation ($\Delta V_{\rm DC}$), and the diesel generator compensates the load increase to restore the voltage of the DC-link to its nominal value.

At $t=20\,\mathrm{s}$, the system is subjected to a wind speed decrease, where the wind speed reduces from 12.5 to 12.3 m/s ($\Delta V_{\mathrm{wind}} = -0.2\,\mathrm{m/s}$). Consequently, the active power supplied by the wind unit is reduced, moving the operating point of the wind turbine from point A to point B, as shown in Fig. 6. The speed of wind turbine is reduced by the MPPT controller so that the new maximum power point can be reached at point C. At the same time, the V_{DC} controller acts to mitigate the voltage variation in the DC-link. Due to the action of the V_{DC} controller, the diesel generator attempts to compensate the deficit of active power in the system and, as a consequence, the rotor of the diesel generator accelerates and the microgrid collapses.

Fig. 11 illustrates the time evolution of some dynamics of the microgrid. This time-domain simulation of the full dynamical model of the microgrid, given by set of equation (5)–(28), was performed by means of a trapezoidal numerical integration

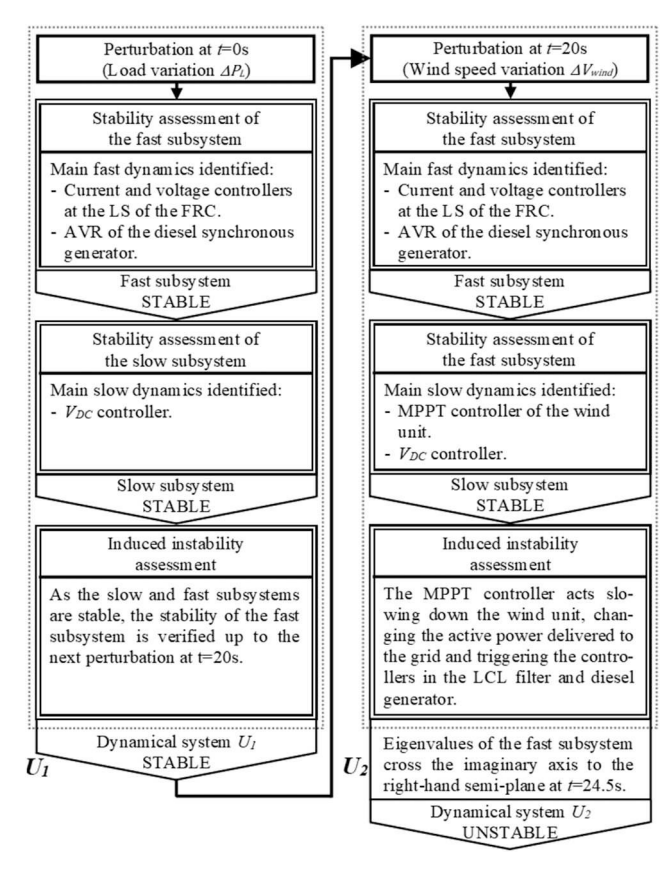


Fig. 9 Flowchart of the sequence of operational events of scenario 1 related to the slow and fast subsystems in the context of time scales

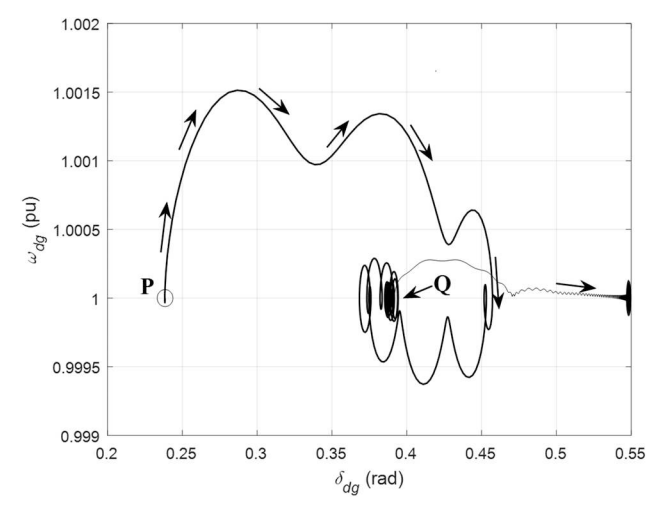


Fig. 10 Phase portrait of δ - ω of the diesel generator from the complete dynamical model of the microgrid

technique [15]. Time-domain simulation indicates that the microgrid is unstable, but it is not clear how the dynamics and microgrids components interact to lead the microgrid into an unstable condition, even more, it is not possible to determine the sequence of events that triggered the instability. The time scale method allows to establish a clear relationship between the dynamics and to detect the mechanisms of collapse of the microgrid. Although the numerical integration of the complete model, given by the set of equation (5)–(28), provides right conclusions regarding the behaviour and stability of the microgrid, there are some drawbacks associated with this approach: (i) need to choose a more sophisticated solver (with higher computational burden) based on variable step-size algorithms to properly perform the numerical integration; (ii) need to use long time intervals of simulations to assess unstable scenarios.

Moreover, variable step-size algorithms are subject to failures due to numerical instability induced by fast dynamics [29]. Also,

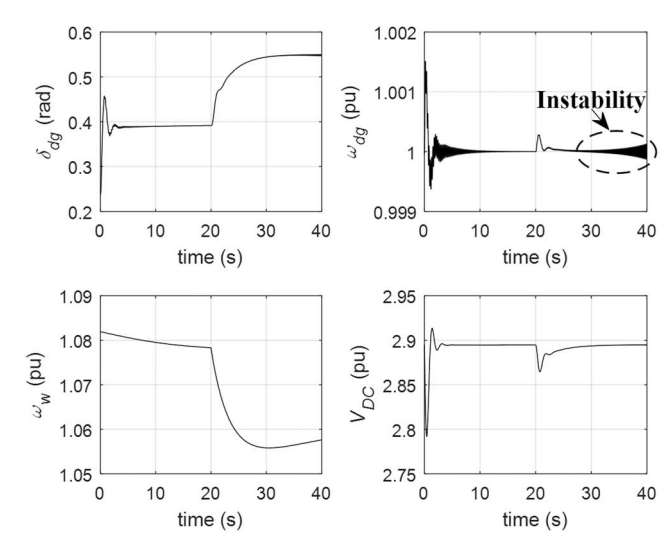


Fig. 11 Evolution of some dynamics of the wind generation based microgrid

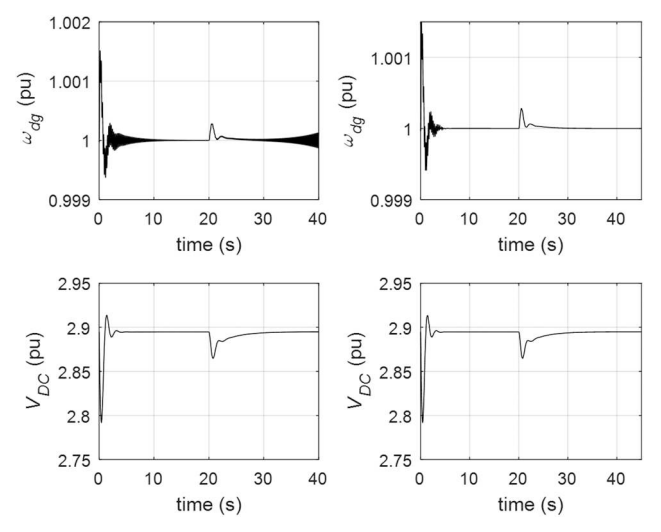


Fig. 12 Numerical simulation of the complete model (Σ_c). Left column: via trapezoidal numerical algorithm; right column: via ode23s from MATLAB[©]

the coexistence of dynamics in very different time ranges often leads to numerical issues and erroneously stability assessment which are dependent on the employed solver. For example, the use of ode23s from MATLAB[©], erroneously indicated stable behaviour when, in reality, the scenario 1 of Table 2 is unstable, as illustrated in Fig. 12, where the time evolution of some dynamics obtained with the ode23s solver clearly shows a wrong numerical response of the dynamics. Time scale analysis, by contrast, mitigates the numerical issues by splitting the model into slow and fast models, improving the numerical stability of the dynamical system simulation [10].

4.2 Stability assessment of scenario 2

In this scenario, the stability analysis is focused on a Hopf bifurcation caused by a system load variation. The microgrid operates at the maximum power point of the wind turbine, point C illustrated in Fig. 6, with $V_{\rm wind,2}$ = 12.2 m/s. In this scenario, the initial operating point of the systems corresponds to the ASEP $(x_{0,2},z_{0,2})$, whose values are presented in Appendix 2. At t = 0 s, a sudden load increase (ΔP_L) equal to 28.52 kW occurs, originating a new dynamical system U_1 . In the dynamical system U_1 , after the load increase, a voltage drop occurs at the load bus, which forces a sudden drop in v_0 and increase in i_i . The variables v_0 and i_i , respectively, correspond to the voltage and current of the LCL filter. This voltage variation results in the action of the controllers of the LS converter and reactive power controller of the diesel

Table 4 Fast subsystem eigenvalues of the dynamical system U_1 of scenario 2

- 7		
Time		
0.1 s	0.3 s	0.4 s
-4949.51 + 34,556.4	7i -4950.34 + 34,553.90i	-4950.77 + 34,552.57i
-4949.51 - 34,556.4	7i –4950.34 – 34,553.90i	-4950.77 - 34,552.57i
-4901.28 + 34,131.20	6i −4901.12 + 34,127.78i	-4901.04 + 34,125.94i
-4901.28 - 34,131.20	6i -4901.12 - 34,127.78i	-4901.04 - 34,125.94i
-6103.21 + 1232.89i	-6102.74 + 1230.82i	-6102.51 + 1229.76i
-6103.21 - 1232.89i	-6102.74 - 1230.82i	-6102.51 - 1229.76i
-80.3409 + 369.784i	-80.534 + 369.641i	-80.629 + 369.561i
-80.3409 - 369.784i	-80.534 - 369.641i	-80.629 - 369.561i
-17.4758 + 49.9969i	0.0971 + 30.744i	0.2047 + 31.1047i
-17.4758 - 49.9969i	0.0971 - 30.744i	0.2047 - 31.1047i
-0.0741 + 30.0705i	-17.655 + 49.481i	-17.769 + 49.207i
-0.0741 - 30.0705i	-17.655 - 49.481i	-17.769 - 49.207i
-2.72848 + 0.0264i	-2.72865 + 0.0253i	-2.7287 + 0.0247i
-2.72848 - 0.0264i	-2.72865 - 0.0253i	-2.7287 - 0.0247i
-20.0171 + 0.00066i	-20.0170 + 0.00064i	-20.0170 + 0.00063i
-20.0171 - 0.00066i	-20.0170 - 0.00064i	-20.0170 - 0.00063i

generator in order to restore the system voltage. These voltage and current variations are fast dynamics related to $(\Pi^{U_1}_{F,2}(\mathbf{x}))$, which bring the microgrid from the point $(\mathbf{x}_{0,2},\mathbf{z}_{0,2})$ to the ASEP of the fast subsystem $(\mathbf{x}_{0,2},\mathbf{z}^*_{0,2})$ at t=0.1 s. The time-scale algorithm proposed in [11] classifies the fast subsystem U_1 as stable, and then the algorithm proceeds with the stability analysis of the slow subsystem U_1 .

The search for an ASEP of the slow subsystem returns ($x_{s_{1},2}^{U_{1}}$ $z_{s_{1,2}}^{U_1}$), and the time-scale algorithm classifies the slow subsystem as stable. The slow subsystem evolution is related to the active power unbalance at the DC-link, causing a slow variation at the DC-link voltage (V_{DC}) . The restoration of the DC-link voltage is a slow process, since this control process involves the action of the diesel engine, synchronous generator of the diesel unit and other components of the wind unit. The synchronous generator of the wind unit does not respond to this perturbation, since the wind turbine operates at the maximum power point and cannot provide additional active power to the system. Thus, only the diesel unit supplies the deficit of energy to restore the voltage at the DC-link bus and recover the stability of the microgrid. Since both dynamical subsystems (fast and slow) were classified as stable by the algorithm in [11], the analysis proceeds to the algorithm presented in Fig. 1. Since there are no more new perturbations, then the stability of the equilibrium of the fast subsystem is monitored along the trajectory of the slow subsystem $(\boldsymbol{\varphi}_{0,2}^{U_1})$.

The eigenvalues of the Jacobian matrix corresponding to the fast subsystem U_1 are used as a tool to monitor the stability of the fast subsystem throughout the trajectory of the slow subsystem of U_1 . At t=0.3 s, this analysis shows, as presented in Table 4, that a pair of conjugate eigenvalues of the fast subsystem cross the imaginary axis of the complex plane to the right-half complex plane, indicating that the equilibrium point of the fast subsystem becomes unstable. As a consequence, the instability of the fast subsystem implies instability of the microgrid.

Fig. 13 illustrates how the QSS analysis (slow simulation) fails in detecting the instability of the wind microgrid after the load variation at t = 0 s. In addition, Fig. 14 illustrates the sequence of the operational events of the microgrid in the context of time scales, pointing out the action of the controllers and devices related to the slow and fast subsystems of the corresponding dynamical system U_1 .

5 Conclusion

Time scale approach is a promising tool for stability analysis of power systems capable of filling the gap of conventional stability

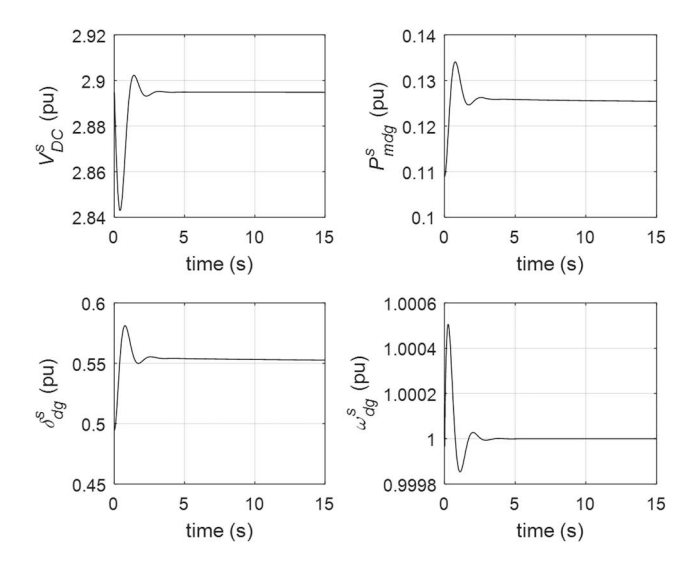


Fig. 13 Numerical simulation of the QSS system for scenario 2

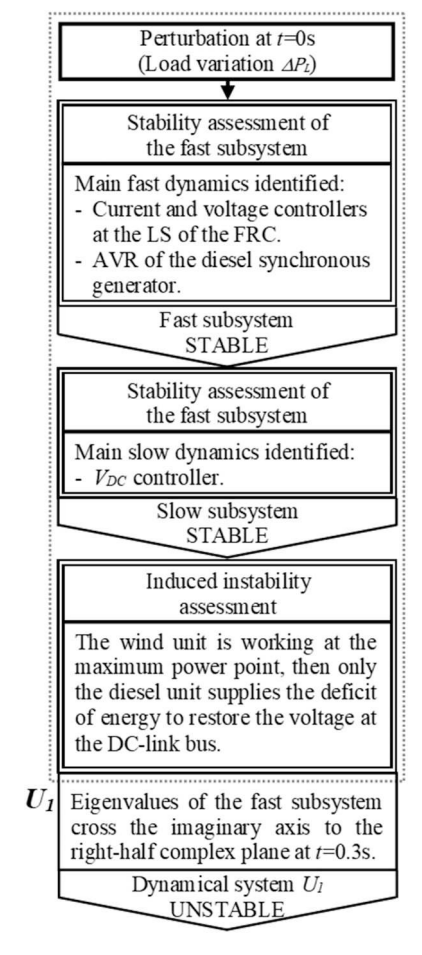


Fig. 14 Flowchart of the sequence of operational events of scenario 2 related to the slow and fast subsystems in the context of time scales

analysis, improving the numerical stability and speeding up the computational analysis of power systems without neglecting the physical interaction between their dynamics. In such context, this paper presents, as one of the main contributions, the application of the time scale method to the analysis of a microgrid based on wind generation. The assessment has been performed by a proposed time scale algorithm for stability analysis of power systems. The proposed time scale algorithm, which is also an innovative contribution of this work, splits the stability analysis of a power system, bridging the gap between short- and mid-term stability analysis.

The successful application of the time scale method to a microgrid based on wind generation provides a deeper insight into

the multiple dynamics inherent to the system and represents a new step in the effort to introduce the time scale method in the stability analysis of modern power systems. In the simultaneous analysis of the fast and slow subsystems, a procedure to detect induced instability of the fast subsystem along the trajectory of the slow dynamical system was proposed. A correct assessment of stability of the microgrid was carried out with clear indication of the dynamic mechanisms of system collapse. This mechanism involves the occurrence of a Hopf bifurcation in the fast subsystem that is triggered by slow changes in the slow dynamics. This is a consequence of interaction between the fast dynamics of interface converters of the wind power generator with electromechanical

The main future directions of this research are: (i) introduce time scale stability analysis in microgrids with more detailed models of static converters, where the inclusion of non-linearities and parasitic parameters can lead to numerical instability; (ii) propose a stability assessment approach based on direct methods, such as the controlling unstable equilibrium point method, in conjunction with time scale approach to deal with microgrids and even larger complex power systems.

6 Acknowledgments

The authors acknowledge São Paulo Research Foundation (FAPESP) (grant #2018/20104-9), FINEP, SETI, CNPq and Fundação Araucária for scholarships and funding. This study was also financed in part by the Coordenação de Aperfeiçoamento de Pessoal de Nível Superior – Brasil (CAPES) – Finance Code 001.

7 References

- Yaramasu, V., Wu, B.: 'Model predictive control of wind energy conversion [1]
- systems' (Wiley-IEEE Press, USA, 2016, 1st edn.)
 Yaramasu, V., Wu, B., Sen, P.C., et al.: 'High-power wind energy conversion systems: state-of-the-art and emerging technologies', Proc. IEEE, 2015, 103, [2]
- [3] Sebastián, R.: 'Battery energy storage for increasing stability and reliability of an isolated wind diesel power system', IET Renew. Power Gener., 2017, 11, (2), pp. 296-303
- Fu, Q., Nasiri, A., Bhavaraju, V., et al.: 'Transition management of microgrids [4] with high penetration of renewable energy', IEEE Trans. Smart Grid, 2014, 5, (2), pp. 539–549
- [5] Anaya-Lara, O., Jenkins, N., Ekanayake, J., et al.: 'Wind energy generation: modelling and control' (John Wiley & Sons Ltd, USA, Chichester, UK, 2009)
- Ma, F., Fu, L.: 'Principle of multi-time scale order reduction and its application in AC/DC hybrid power systems'. Int. Conf. on Electrical Machines and Systems, Wuhan, China, October 2008, pp. 3951–3956 Kallamadi, M., Sarkar, V.: 'Generalised analytical framework for the stability
- [7] studies of an AC microgrid', IET The J. Eng., 2016, 2016, (6), pp. 171-179
- Davarani, R.Z., Ghazi, R., Pariz, N.: 'Non-linear analysis of DFIG based wind farm in stressed power systems', IET Renew. Power Gener., 2014, 8, (8), pp.
- Lukasievicz, T., Oliveira, R.V., Torrico, C.: 'A control approach and [9] supplementary controllers for a stand-alone system with predominance of wind generation', *Energies*, 2018, **11**, (411), pp. 1–17
- Xu, X., Jia, H., Chiang, H.-D., et al.: 'Dynamic modeling and interaction of hybrid natural gas and electricity supply system in microgrid', IEEE Trans. Power Syst., 2015, 30, (3), pp. 1212–1221
- [11] Choque Pillco, E., Alberto, L.F.C.: 'On the foundations of stability analysis of power systems in time scales', IEEE Trans. Circuits Syst. I, Regul. Pap., 2015, **62**, (5), pp. 1230–1239 Jafarian, M., Ranjbar, A.M.: 'Interaction of the dynamics of doubly fed wind
- [12] generators with power system electromechanical oscillations', IET Renew. Power Gener., 2013, 7, (2), pp. 89–97
 Yang, D., Ajjarapu, V.: 'A decoupled time-domain simulation method via
- invariant subspace partition for power system analysis', IEEE Trans. Power Syst., 2006, 21, (1), pp. 11–18
- Jardim, J., de Oliveira Salim, K.C., dos Santos, P.H.L., et al.: 'Variable time step application on hybrid eletromechanical-eletromagnetic simulation', IET Gener. Transm. Distrib., 2017, 11, (12), pp. 2968-2973
- Sauer, P.W., Pai, M.A., Chow, J.H.: 'Power system dynamics and stability: with synchrophasor measurement and power system toolbox' (Wiley-IEEE
- Press, USA, 2017, 2nd edn.) Wang, X., Chiang, H.-D.: 'Quasi steady-state model for power system [16] stability: limitations, analysis and a remedy'. Power Systems Computation Conf., Wroclaw, Poland, August 2014
- Kuehn, C.: 'Multiple time scale dynamics' (Springer, Bern, Switzerland,
- Chiang, H.-D., Alberto, L.F.C.: 'Stability regions of nonlinear dynamical systems: theory, estimation, and applications' (Cambridge University Press, UK, 2015, 1st edn.)

- Li, Y., Yang, Z., Li, G., et al.: 'Optimal scheduling of an isolated microgrid with battery storage considering load and renewable generation uncertainties'
- IEEE Trans. Ind. Electron., 2019, 66, (2), pp. 1565-1575
 Tang, Y., Ye, H., Kong, L., et al.: 'Multi-scale transient modeling and realtime simulation of AC/DC power grid with multi-terminal VSC-HVDC'. IEEE Conf. on Energy Internet and Energy System Integration (EI2), Beijing, China, November 2017
- Modi, N., Tapan, K.S., Mithulananthan, N.: 'Effect of wind farms with doubly fed induction generators on small-signal stability – a case study on Australian equivalent system'. IEEE PES Innovative Smart Grid Technologies, Perth, Australia, November 2011
- Pogaku, N., Prodanovic, M., Green, T.C.: 'Modeling, analysis and testing of autonomous operation of an inverter-based microgrid', IEEE Trans. Power Electron., 2007, 22, (2), pp. 613-625
- [23] Quéval, L., Ohsaki, H.: 'Back-to-back converter design and control for synchronous generator-based wind turbines'. Int. Conf. on Renewable Energy Research and Applications (ICRERA), Nagasaki, Japan, November 2012 Huang, H., Mao, C., Lu, J., et al.: 'Small-signal modelling and analysis of
- wind turbine with direct drive permanent magnet synchronous generator connected to power grid', IET Renew. Power Gener., 2012, 6, (1), pp. 48-58
- Das, D., Aditya, S.K., Kothari, D.P.: 'Dynamics of diesel and wind turbine generators on an isolated power system', Int. J. Electr. Power Energy Syst., 1999, **21**, (3), pp. 183–189
- Kwatny, H.G., Miu-Mille, K.: 'Power system dynamics and control' (Springer, Birkhäuser, USA, 2016, 1st edn.) [26]
- Vahdati, P.M., Kazemi, A., Hadi Amini, M., et al.: 'Hopf bifurcation control of power system nonlinear dynamics via a dynamic state feedback controllerpart I: theory and modeling', IEEE Trans. Power Syst., 2017, 32, (4), pp. 3217-3228
- Hemmatpour, M.H., Mohammadian, M., Gharaveisi, A.-A.: 'Simple and efficient method for steady-state voltage stability analysis of islanded microgrids with considering wind turbine generation and frequency deviation', IET Gener. Transm. Distrib., 2016, 10, (7), pp. 1691-1702
- Chang, Y., Yu, J.: 'A long term dynamic simulation method of power system based on variables grouping and seceding grouping strategy'. Third Int. Conf. on Electric Utility Deregulation and Restructuring and Power Technologies, Nanjing, China, April 2008, pp. 1077-1081

Appendix

8.1 Appendix 1: instability theorem demonstration

The following general hypothesis are made for the singularly perturbed system (\sum_{ε}) : (H1) All the equilibrium points are hyperbolic. (H2) Every bounded trajectory approaches an equilibrium point. Hypothesis (H1) is a generic property of vector fields and the existence of an energy function [18] is a sufficient condition that guarantees (H2).

Theorem 1: Consider the singularly perturbed system (Σ_{ε}) and their corresponding subsystems (Π_F) and (Σ_0) satisfying hypotheses (H1)-(H2) for sufficiently small $\varepsilon > 0$. Let (x_s, z_s) be a hyperbolic ASEP of (Σ_{ε}) and $A_{\varepsilon}(x_{\rm S},z_{\rm S})$ be its stability region (SR). Suppose $(x_0,z_0) \notin A_F(\Gamma_s)$, then:

- (i) If $\Phi_0(\tau,x_0,z_0)$ is bounded, then there exists $(x_0,z^*) \in \Gamma_{s1} \neq \Gamma_s$ such that $\Phi_0(\tau,x_0,z_0) \to (x_0,z^*)$ as $\tau \to \infty$, and: (i.1) If $\varphi_0(\tau,x_0,z^*)$ is bounded, then $(x_0,z_0) \notin A_{\varepsilon}(x_s,z_s)$ for sufficiently small $\varepsilon > 0$. (i.2) If $\varphi_0(\tau,x_0,z^*)$ is unbounded, then for every M>0, there exists T>0and $\varepsilon^* > 0$ such that $||\varphi_0(T, x_0, z_0)|| > M \forall \varepsilon \in (0, \varepsilon^*)$, that is, || $\varphi_{\varepsilon}(t,x_0,z_0)||$ assumes large values for sufficiently small ε .
- (ii) If $\Phi_0(\tau, \mathbf{x}_0, \mathbf{z}_0)$ is unbounded, then for every M > 0, there exists T > 0 and $\varepsilon * > 0$ such that $||\Phi_{\varepsilon}(T, \mathbf{x}_0, \mathbf{z}_0)|| > M \ \forall \varepsilon \in (0, \varepsilon^*)$, that is $||\mathbf{x}_0|| < \infty$ $\Phi_{\varepsilon}(\tau, x_0, z_0)$ || assumes large values for sufficiently small ε .

Proof: Let $(x_0,z_0) \notin A_F(\Gamma_s)$, then two possibilities can occur for the solution $\Phi_0(\tau,x_0,z_0)$ of $(\Pi_F(x_0))$. Either (i) $\Phi_0(\tau,x_0,z_0)$ is bounded for $(0,\omega_+)$, with ω_+ being the maximal time of existence (to the right) of the solution $\Phi_0(\tau_*x_0,z_0)$ or (ii) $||\Phi_0(\tau_*x_0,z_0)||\to\infty$ as $\tau \to \omega_+$. In case (i), hypothesis (H2) for (Π_F) guarantees $\omega_+ = \infty$ and $\Phi_0(\tau,x_0,z_0) \to (x_0,z^*) \in \Gamma_{s1} \neq \Gamma_s$ as $\tau \to \infty$. Now we have two subcases: (i.1) If $\varphi_0(x_0,z^*)$ is bounded and $(x_0,z^*) \in A_F(\Gamma_{s1})$, hypothesis (H2) for (Σ_0) guarantees $\varphi_0(t,x_0,z^*) \rightarrow (x_{eq},z_{eq})$ as $t \rightarrow$ ∞ , where (x_{eq}, z_{eq}) is an ASEP on Γ_{s1} . Thus, $(x_0, z^*) \in A_0(x_{eq}, z_{eq})$ for sufficiently small $\varepsilon > 0$, thus, Theorem 2 in [16] implies (x_0, z_0)

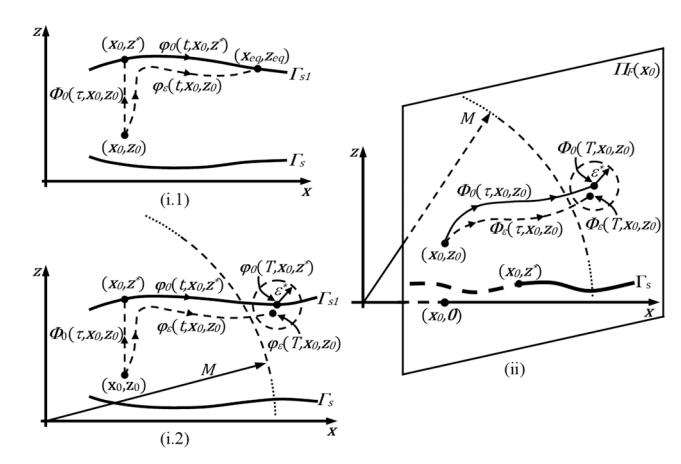


Fig. 15 Geometrical interpretation of the proof of Theorem 1. Three cases were considered to explain the instability of (Σ_c) due to the instability of (Π_F)

 $\in A_{\varepsilon}(x_{\mathrm{eq}},z_{\mathrm{eq}})$ for sufficiently small $\varepsilon>0$, that is, $(x_0,z_0)\notin A_{\varepsilon}(x_s,z_s)$ for sufficiently small $\varepsilon>0$. (i.2) If $\varphi_0(x_0,z^*)$ is unbounded, then for every M>0, there exists T>0 such that $||\varphi_0(T,x_0,z^*)||>M+\mu$ with $\mu>0$. Tikhonov's theorem for a finite interval of time [0,T] guarantees the existence of sufficiently small $\varepsilon^*>0$ such that $||\varphi_\varepsilon(T,x_0,z_0)||>M \ \forall \varepsilon\in(0,\ \varepsilon^*)$ [8]. In case (ii), for every M>0, there exists T>0 such that $||\Phi_0(T,x_0,z_0)||>M+\mu$ with $\mu>0$. From the continuity of solutions with respect to initial states and parameters theorem [17], for $(\Pi_F(x_0))$ guarantees the existence of sufficiently small $\varepsilon^{**}>0$ such that $\Phi_\varepsilon(T,x_0,z_0)>M \ \varepsilon\in(0,\varepsilon^{**})$. This completes the proof. \square

Theorem 1 establishes that the instability of (Π_F) implies instability of (Σ_c) . Fig. 15 is a geometrical interpretation of Theorem 1. Scenario (i.1) illustrates the case in which the initial condition (x_0,z_0) is outside the SR of the stable equilibrium point of interest and converges to another equilibrium point in a different constraint manifold. Scenario (i.2) illustrates the case in which the system trajectories are unbounded in the direction of the slow dynamics. Scenario (ii) illustrates the case when the trajectories are unbounded due to fast dynamics.

8.2 Appendix 2: asymptotically stable equilibrium points

The values of the ASEPs of the scenario 1 are presented below:

 $\begin{array}{l} (\mathbf{x}_{0,1}, \mathbf{z}_{0,1}) = (U_{eow} = 2.5657, \ U_{eidw} = 0.0, \ U_{eiqw} = 0.0, \ \omega_{wr} = 1.0768, \\ \omega_{w} = 1.0819, \ E_{fdw} = 0.9903, \ i_{dw} = 0.0, \ i_{qw} = 0.7877, \ i_{fw} = 0.8059, \\ U_{eVDC} = -0.0338, \ V_{DC} = 2.8949, \ P_{mdg} = 0.0485, \ \delta_{dg} = 0.2385, \ \omega_{dg} = 1.0, \ U_{evod} = 0.0188, \ U_{evoq} = -0.0036, \ U_{eiid} = 0.0009, \ U_{eiiq} = 0.0, \\ i_{id} = 0.7606, \ i_{iq} = -0.1002, \ v_{od} = 1.01, \ v_{oq} = 0.0, \ i_{od} = 0.7606, \ i_{oq} = -0.146, \ E_{fddg} = 1.3569, \ i_{ddg} = 0.0313, \ i_{qdg} = 0.0406, \ i_{fdg} = 0.132). \\ (\mathbf{x}_{0.1}, \ \mathbf{z}_{0.1}^*) = (U_{eow} = 2.5657, \ U_{eidw} = 0.0, \ U_{eiqw} = 0.0, \ \omega_{wr} = 1.0768, \\ \omega_{w} = 1.0819, \ E_{fdw} = 0.9903, \ i_{dw} = 0.0, \ i_{qw} = 0.7877, \ i_{fw} = 0.8059, \\ U_{eVDC} = -0.0338, \ V_{DC} = 2.8949, \ P_{mdg} = 0.0485, \ \delta_{dg} = 0.2388, \ \omega_{dg} = 0.2388,$

 $= 1.0, \ U_{evod} = 0.0196, \ U_{evoq} = -0.0040, \ U_{eiid} = 0.0009, \ U_{eiiq} = 0.0,$ $i_{id} = 0.791$, $i_{iq} = -0.1139$, $v_{od} = 1.01$, $v_{oq} = 0.0$, $i_{od} = 0.791$, $i_{oq} = 0.791$ -0.159, $E_{fddg} = 1.356$, $i_{ddg} = 0.0314$, $i_{qdg} = 0.041$, $i_{fdg} = 0.1319$). $(\mathbf{x}_{s_{1,1}}^{U_{1}}, \mathbf{z}_{s_{1,1}}^{U_{1}}) = (U_{e\omega w} = 2.6183, U_{eidw} = 0.0, U_{eiqw} = 0.0, \omega_{wr} = 1.0776$ $\omega_w = 1.0777$, $E_{fdw} = 0.9823$, $i_{dw} = 0.0$, $i_{qw} = 0.7857$, $i_{fw} = 0.81$, $U_{e\text{VDC}} = 0.026$, $V_{DC} = 2.8947$, $P_{mdg} = 0.0828$, $\delta_{dg} = 0.3928$, $\omega_{dg} = 0.3928$ 1.0, $U_{evod} = 0.0188$, $U_{evog} = -0.0039$, $U_{eiid} = 0.0009$, $U_{eiiq} = 0.0$, i_{id} = 0.7595, i_{iq} = -0.1118, v_{od} = 1.01, v_{oq} = 0.0, i_{od} = 0.7595, i_{oq} = -0.158, $E_{fddg} = 1.515$, $i_{ddg} = 0.0479$, $i_{qdg} = 0.0654$, $i_{fdg} = 0.1474$). $(x_{1,1},z_{1,1}) = (U_{e\omega w} = 2.612, \ U_{eidw} = 0.0, \ U_{eigw} = 0.0, \ \omega_{wr} = 1.0776,$ $\omega_w = 1.0783$, $E_{fdw} = 0.9851$, $i_{dw} = 0.0$, $i_{qw} = 0.7861$, $i_{fw} = 0.8093$, $U_{eVDC} = 0.0255$, $V_{DC} = 2.8947$, $P_{mdg} = 0.0825$, $\delta_{dg} = 0.3915$, $\omega_{dg} = 0.0825$ 1.0, $U_{evod} = 0.0188$, $U_{evog} = -0.0039$, $U_{eiid} = 0.0009$, $U_{eiiq} = 0.0$, i_{id} = 0.7598, i_{iq} = -0.1118, v_{od} = 1.01, v_{oq} = 0.0, i_{od} = 0.7598, i_{oq} = -0.158, $E_{fddg} = 1.513$, $i_{ddg} = 0.0478$, $i_{qdg} = 0.0652$, $i_{fdg} = 0.1472$). $(\mathbf{x}_{1,1}, \mathbf{z}_{1,1}^*) = (U_{e\omega w} = 2.612, U_{eidw} = 0.0, U_{eiqw} = 0.0, \omega_{wr} = 1.0776,$ $\omega_w = 1.0783$, $E_{fdw} = 0.9851$, $i_{dw} = 0.0$, $i_{qw} = 0.7861$, $i_{fw} = 0.8093$, $U_{e\text{VDC}} = 0.0255, V_{DC} = 2.8947, P_{mdg} = 0.0825, \delta_{dg} = 0.3915, \omega_{dg} = 0.0825, \delta_{dg} = 0.0825$ 1.0, $U_{evod} = 0.0188$, $U_{evoq} = -0.0039$, $U_{eiid} = 0.0009$, $U_{eiiq} = 0.0$, i_{id} = 0.7598, i_{iq} = -0.1118, v_{od} = 1.01, v_{oq} = 0.0, i_{od} = 0.7598, i_{oq} = -0.158, $E_{fddg} = 1.513$, $i_{ddg} = 0.0478$, $i_{qdg} = 0.0652$, $i_{fdg} = 0.1472$). $(\mathbf{x}_{sz,1}^{U_2}, \mathbf{z}_{sz,1}^{U_2}) = (U_{e\omega w} = 2.4787, U_{eidw} = 0.0000, U_{eiqw} = 0.0000, \omega_{wr}$ = 1.00604, ω_w = 1.0592, E_{fdw} = 0.9886, i_{dw} = 0.0, i_{qw} = 0.7394, i_{fw} = 0.8337, U_{eVDC} = 0.0971, V_{DC} = 2.8948, P_{mdg} = 0.1235, δ_{dg} = 0.5466, $\omega_{dg} = 1.0$, $U_{evod} = 0.0179$, $U_{evoq} = -0.0039$, $U_{eiid} = 0.0009$, $U_{eiiq} = 0.0$, $i_{id} = 0.7234$, $i_{iq} = -0.1103$, $v_{od} = 1.01$, $v_{oq} = 0.0$, $i_{od} = 0.0$ 0.7234, $i_{og} = -0.156$, $E_{fddg} = 1.762$, $i_{ddg} = 0.0742$, $i_{adg} = 0.0897$, $i_{fdg} = 0.0897$ = 0.1714)

The values of the ASEPs of the scenario 2 are presented below:

 $(\mathbf{x}_{0,2}, \mathbf{z}_{0,2}) = (U_{e\omega w} = 2.4203, U_{eidw} = 0.0, U_{eiqw} = 0.0, \omega_{wr} = 1.0519,$ $\omega_w = 1.0495$, $E_{fdw} = 0.9901$, $i_{dw} = 0.0$, $i_{qw} = 0.7175$, $i_{fw} = 0.8458$, $U_{eVDC} = 0.0717$, $V_{DC} = 2.8948$, $P_{mdg} = 0.1089$, $\delta_{dg} = 0.4944$, $\omega_{dg} = 0.4944$ 1.0, $U_{evod} = 0.0175$, $U_{evoq} = -0.0035$, $U_{eiid} = 0.0009$, $U_{eiiq} = 0.0$, i_{id} = 0.7057, i_{iq} = -0.0973, v_{od} = 1.01, v_{oq} = 0.0, i_{od} = 0.7057, i_{oq} = -0.143, $E_{fddg} = 1.668$, $i_{ddg} = 0.0641$, $i_{qdg} = 0.0816$, $i_{fdg} = 0.1622$). $(\mathbf{x}_{0,2}, \mathbf{z}_{0,2}^*) = (U_{e\omega w} = 2.42, U_{eidw} = 0.0, U_{eigw} = 0.0, \omega_{wr} = 1.0519,$ $\omega_w = 1.0495$, $E_{fdw} = 0.9901$, $i_{dw} = 0.0$, $i_{qw} = 0.7175$, $i_{fw} = 0.8458$, $U_{eVDC} = 0.0726$, $V_{DC} = 2.8748$, $P_{mdg} = 0.1107$, $\delta_{dg} = 0.5009$, $\omega_{dg} = 0.5009$ 1.0, $U_{evod} = 0.0178$, $U_{evog} = -0.0037$, $U_{eiid} = 0.0009$, $U_{eiiq} = 0.0$, i_{id} = 0.7192, i_{iq} = -0.1037, v_{od} = 1.01, v_{oq} = 0.0, i_{od} = 0.7192, i_{oq} = -0.149, $E_{fddg} = 1.679$, $i_{ddg} = 0.065$, $i_{qdg} = 0.0826$, $i_{fdg} = 0.1633$). $(\mathbf{x}_{s1,2}^{U_2}, \mathbf{z}_{s1,2}^{U_2}) = (U_{e\omega w} = 2.4010, U_{eidw} = 0.0, U_{eiqw} = 0.0, \omega_{wr} = 0.0)$ 1.0518, $\omega_w = 1.0512$, $E_{fdw} = 0.9958$, $i_{dw} = 0.0$, $i_{qw} = 0.7184$, $i_{fw} = 0.00$ 0.8440, $U_{eVDC} = 0.1003$, $V_{DC} = 2.8948$, $P_{mdg} = 0.1254$, $\delta_{dg} = 0.1254$ $0.5526, \ \omega_{dg} = 1.0, \ U_{evod} = 0.0175, \ U_{evoq} = -0.0037, \ U_{eiid} = 0.0009,$ $U_{eiiq} = 0.0$, $i_{id} = 0.7063$, $i_{iq} = -0.1033$, $v_{od} = 1.01$, $v_{oq} = 0.0$, $i_{od} = 0.0$ 0.7063, $i_{oq} = -0.149$, $E_{fddg} = 1.775$, $i_{ddg} = 0.0754$, $i_{qdg} = 0.0907$, $i_{fdg} = 0.0907$